Available online at www.sciencedirect.com
SCIENCE DIRECT®
Journal of Colloid and Interface Science 270 (2004) 9–20
JOURNAL OF Colloid and Interface Science
www.elsevier.com/locate/jcis

EXAFS study of mercury(II) sorption to Fe- and Al-(hydr)oxides II. Effects of chloride and sulfate

Christopher S. Kim,[a,*] James J. Rytuba,[b] and Gordon E. Brown Jr. [a,c]

[a] *Surface and Aqueous Geochemistry Group, Department of Geological and Environmental Sciences, Stanford University, Stanford, CA 94305-2115, USA*
[b] *U.S. Geological Survey, 345 Middlefield Road, MS 901, Menlo Park, CA 94025, USA*
[c] *Stanford Synchrotron Radiation Laboratory, SLAC, 2575 Sand Hill Rd., MS 99, Menlo Park, CA 94025, USA*

Received 15 September 2002; accepted 18 July 2003

Abstract

Common complexing ligands such as chloride and sulfate can significantly impact the sorption of Hg(II) to particle surfaces in aqueous environmental systems. To examine the effects of these ligands on Hg(II) sorption to mineral sorbents, macroscopic Hg(II) uptake measurements were conducted at pH 6 and $[Hg]_i = 0.5$ mM on goethite (α-FeOOH), γ-alumina (γ-Al_2O_3), and bayerite (β-$Al(OH)_3$) in the presence of chloride or sulfate, and the sorption products were characterized by extended X-ray absorption fine structure (EXAFS) spectroscopy. The presence of chloride resulted in reduced uptake of Hg(II) on all three substrates over the Cl^- concentration ($[Cl^-]$) range 10^{-5} to 10^{-2} M, lowering Hg surface coverages on goethite, γ-alumina, and bayerite from 0.42 to 0.07 μmol/m^2, 0.06 to 0.006 μmol/m^2, and 0.55 to 0.39 μmol/m^2 ($[Cl^-] = 10^{-5}$ to 10^{-3} M only), respectively. This reduction in Hg(II) uptake is primarily a result of the formation of stable, nonsorbing aqueous $HgCl_2$ complexes in solution, limiting the amount of free Hg(II) available to sorb. At higher $[Cl^-]$ beam reduction of Hg(II) to Hg(I) was observed, resulting in the possible formation of aqueous Hg_2Cl_2 species and the precipitation of calomel, $Hg_2Cl_{2(s)}$. The presence of sulfate caused enhanced Hg(II) uptake over the sulfate concentration ($[SO_4^{2-}]$) range 10^{-5} to 0.9 M, increasing Hg surface coverages on goethite, γ-alumina, and bayerite from 0.39 to 0.45 μmol/m^2, 0.11 to 0.38 μmol/m^2, and 0.36 to 3.33 μmol/m^2, respectively. This effect is likely due to the direct sorption or accumulation of sulfate ions at the substrate interface, effectively reducing the positive surface charge that electrostatically inhibits Hg(II) sorption. Spectroscopic evidence for ternary surface complexation was observed in isolated cases, specifically in the Hg–goethite–sulfate system at high $[SO_4^{2-}]$ and in the Hg–goethite–chloride system.

Keywords: EXAFS; Mercury; Sorption; Goethite; γ-Alumina; Bayerite; Chloride; Sulfate

1. Introduction

The sorption of mercury onto particle surfaces can be significantly affected by the presence of complexing ligands [1]. Inorganic ligands prevalent in freshwater and seawater include bicarbonate, carbonate, chloride, phosphate, sulfate, and sulfide, while organic ligands such as amino, carboxylic, fulvic, and humic acids are also common in natural waters [2]. Most ligands will lower or enhance the adsorption of metal cations due to several possible processes including (a) formation of stable nonadsorbing metal–ligand aqueous complexes [1,3–6]; (b) formation of metal–ligand ternary surface complexes, which at high metal and ligand concentrations can lead to surface precipitation [7–11]; (c) competitive ligand sorption to particle surfaces, effectively blocking the more reactive sorption sites at the surface [12,13]; and (d) reduction of the positive charge at mineral surfaces (assuming ligands are anions and pH levels are below the pH_{pzc} of the mineral), thereby lowering the electrostatic repulsion of cations by the surface [10,14–17]. Molecular-scale knowledge of the interactions between Hg(II), complexing ligands, and particles found in natural aquatic systems is therefore necessary for understanding the roles of these ligands in metal-ion sorption processes at mineral–water interfaces. This information is also important in predicting the effect of changes in ligand concentrations on Hg(II) adsorption/desorption processes during Hg transport through different aquatic systems (e.g., from smaller streams and rivers to lakes, bays, and oceans).

* Corresponding author.
E-mail address: chriskim@pangea.stanford.edu (C.S. Kim).

0021-9797/$ – see front matter
doi:10.1016/j.jcis.2003.07.029

A number of uptake studies have investigated Hg(II) sorption onto various substrates (see references listed herein and in [18]), with several focusing on Fe- and Al-(hydr)oxides due to their abundance in natural systems and their effectiveness as sorbents for Hg(II). Some of these studies have also explored the macroscopic influences of complexing ligands on sorption, typically investigating the effects of chloride. Chloride is ubiquitous in marine systems, where $[Cl^-]$ averages $10^{-0.3}$ M [2], as well as in hot-spring Hg depositional environments, where $[Cl^-]$ of $10^{-1.2}$ M has been observed [19]. However, chloride can affect Hg(II) adsorption to mineral surfaces at much lower concentrations as well, with reductions in Hg(II) uptake to goethite (α-FeOOH) observed at $10^{-5.3}$ M $[Cl^-]$ [4]. Several studies have reported a shift in the macroscopic Hg(II) adsorption edge to higher pH levels as a function of $[Cl^-]$, indicating that Hg(II) sorption is inhibited as $[Cl^-]$ increases [4,5,20]. This inhibition is considered to be due to the formation of $HgCl_{2(aq)}$ complexes, which are stable in solution and less prone to sorption [6,21].

Another important complexing ligand is sulfate, with average concentrations of $10^{-3.9}$ M in rivers and $10^{-1.5}$ M in oceans [22]. In acid mine drainage (AMD) environments, where oxidation of sulfide minerals generates high concentrations of sulfuric acid, $10^{-0.5}$ M $[SO_4^{2-}]$ has been measured in Hg mine drainage waters [23] and can be as high as 7.9 M in extreme AMD systems such as Iron Mountain, CA [24]. Sulfate has been shown to enhance Pb(II) [10], Cd(II) [14], and Cu(II) [25] uptake onto goethite. Recent studies have found sulfate to have no effect on Hg(II) sorption onto kaolinite [26] and to slightly reduce Hg(II) sorption onto manganese oxide, gibbsite, and quartz [27,28]. However, to the authors' knowledge only a few studies [10,15,16] have used spectroscopic methods to determine the effects of ligands such as chloride and sulfate on heavy metal sorption, and only one known study [29] has explored ternary Hg(II)–chloro complexes on mineral surfaces using a spectroscopic approach.

The objective of this study is to determine how the sorption of Hg(II) from aqueous solution onto goethite, γ-alumina (γ-Al_2O_3), and bayerite (β-$Al(OH)_3$) is impacted by the presence of chloride and sulfate. This paper is the second of a two-part study investigating the sorption of Hg(II) onto Fe- and Al-(hydr)oxides. In Part I [18], the sorption of Hg(II) on these substrates was characterized as a function of pH using a combination of uptake measurements, EXAFS spectroscopy, and bond valence analysis. That study demonstrated that Hg(II) sorbs strongly as a bidentate corner-sharing surface complex to the $Fe(O,OH)_6$ octahedra of the goethite structure and equally strongly but as monodentate, corner-sharing bidentate, and edge-sharing bidentate complexes to the $Al(O,OH)_6$ octahedra that compose the bayerite structure. Hg(II) was found to sorb weakly to γ-alumina, perhaps due to the conversion of the hydrated γ-alumina surface to a secondary bayerite-like phase. Additionally, beam reduction of Hg(II) to Hg(I) in this system resulted in the formation of Hg(I) dimers that appear to sorb weakly to the hydrated γ-alumina surface as monodentate and bidentate corner-sharing complexes. The Hg sorption products in these model systems were found to be similar to those on natural fine-grained Fe- and Al-(hydr)oxide materials from Hg-mine sites, supporting the use of synthetic mineral powders as simplified surrogates for natural environmental substrates. These results serve as a baseline for comparison with those from the ligand-bearing systems in the present study.

2. Experimental methods

Mineral substrates used in uptake experiments were prepared (goethite) or purchased (γ-alumina, bayerite) as described in the previous study [18]; surface areas as determined through BET analysis were 91, 97, and 9 m^2/g, respectively. Batch uptake experiments were mostly conducted in a 0.1 M $NaNO_3$ solution with N_2 gas bubbling through the sample vessels throughout the course of the experiments to minimize contamination from CO_2 and other gases. The solution was then equilibrated with the desired concentration of chloride or sulfate using prepared solutions of reagent grade NaCl and Na_2SO_4 dissolved in water from a NANOpure Infinity water purification system. For ligand concentrations $\geqslant$0.1 M (sulfate experiments only), no $NaNO_3$ was added to the solution. Initial chloride concentrations ranged from 10^{-5} to 10^{-2} M, while initial sulfate concentrations ranged from 10^{-5} to 0.9 M. Aqueous speciation diagrams of the experimental conditions for the chloride- and sulfate-bearing sorption systems are shown in Figs. 1 and 2, respectively. A mass of 0.5 g of solid was suspended in a final volume of 50 ml, resulting in a solids concentration of 10 g/l. For the γ-alumina sorption experiments conducted in the presence of sulfate, 0.25 g of solid was used to minimize the substrate dissolution observed in Part I [18].

Each suspension was titrated to pH 4 using 20-µl aliquots of 0.1 M HNO_3 before 5 ml of a 5 mM $Hg(NO_3)_2$ Mallinckrodt stock solution (Lot 4737) was added to achieve a final solution concentration of 0.5 mM Hg(II). Such high concentrations of Hg(II) were necessary to ensure sufficient Hg(II) uptake onto the substrates for adequate EXAFS analysis. While the experimental Hg(II) concentration greatly exceeds those observed in natural systems, it is not expected to significantly impact the method of uptake since the final Hg(II) concentration is too low to induce precipitation (e.g., of $HgO_{(s)}$, $HgCl_{2(s)}$). Using 20-µl aliquots of 0.1 M NaOH, the pH was titrated to 6.0 and the final volume brought up to 50 ml. Samples were capped and equilibrated on a rotator for a minimum of 24 h before analysis.

Following equilibration, samples were centrifuged at 15,000 RPM for 15 min and the supernatants separated from the solids. The final pH levels of the supernatants were measured prior to filtration with a 0.45-µm filter and acidification to pH < 2 using concentrated HNO_3. All su-

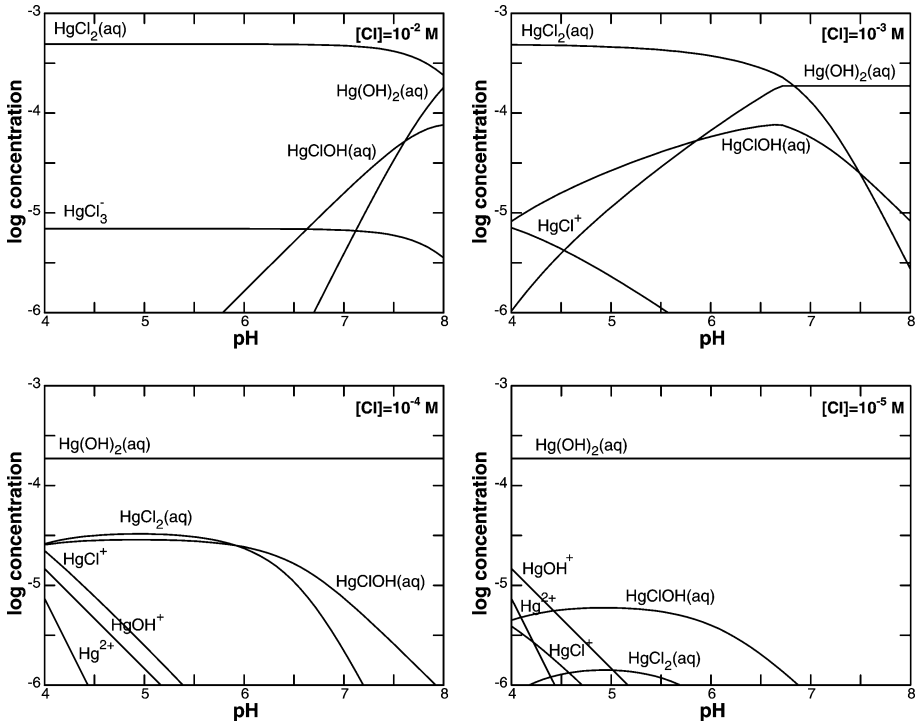

Fig. 1. Aqueous speciation diagrams of Hg (initial Hg(II) concentration = 0.5 mM) in the presence of chloride. See Fig. 2 for the aqueous speciation of Hg(II) in the absence of complexing ligands. Stability constants from Martell and Smith [48] were used in constructing the diagrams.

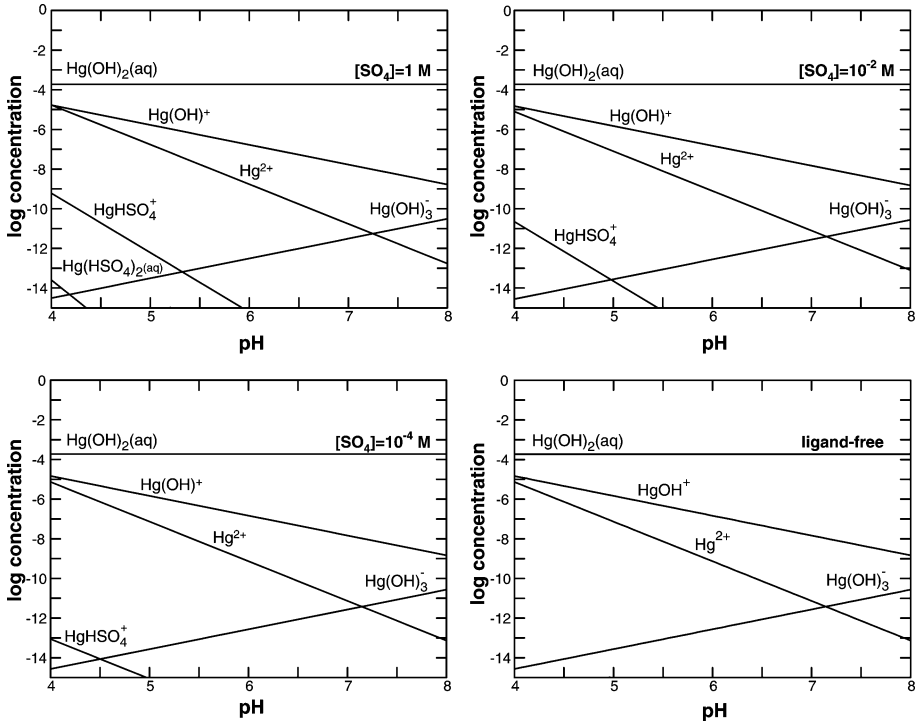

Fig. 2. Aqueous speciation diagrams of Hg (initial Hg(II) concentration = 0.5 mM) in the presence of sulfate and in ligand-free systems. Stability constants from Martell and Smith [48] were used in constructing the diagrams.

pernatants were analyzed for Hg(II) using a TJA IRIS Advantage/1000 Radial inductively coupled plasma (ICP) spectrometer. From these measurements, the degree of Hg(II) uptake to the solids was calculated assuming no significant loss to the sample vessel walls, as verified through control samples.

Sorption products were loaded as moist pastes into sample holders and analyzed using EXAFS spectroscopy. All

EXAFS data were collected at the Stanford Synchrotron Radiation Laboratory (SSRL) on wiggler-magnet beamline 4-3 using Si(111) or Si(220) monochromator crystals. HgL_{III}-edge EXAFS spectra were collected on the sorption samples at room temperature in the fluorescence-yield mode using a 13-element high-throughput germanium detector. This method is optimized for low-concentration samples [30] and enabled collection of HgL_{III}-EXAFS spectra from the sorption products generated. Arsenic and aluminum filters served to attenuate elastic scattering and background matrix fluorescence, respectively. EXAFS data were processed using the EXAFSPAK data analysis software package [31]. Phase and amplitude functions for quantitative fitting were generated from model structures using FEFF 7.0 [32].

EXAFS spectra were fit by (a) isolating and fitting the first-shell Fourier transform feature to provide starting values for coordination number (CN), interatomic bond distance (R), and energy shift (E_0); (b) isolating and fitting the second and/or more distant Fourier transform features using the E_0 value derived from the first-shell fitting; and (c) fitting the complete background-subtracted, k^3-weighted EXAFS spectra using the CN, R, and E_0 values from the filtered fitting steps as the initial values of these variables. The scale factor (S_0) was fixed at 0.9 for all samples based on previous experience in fitting well-characterized crystalline model compounds in which the scale factor was allowed to vary during fitting. The Debye–Waller factor, which serves as a measure of thermal vibration and static disorder around Hg in the sample, was typically allowed to float when fitting the first shell but otherwise set at values appropriate to those of sorption complexes (0.005 for first-shell atomic neighbors, 0.01 for second- and third-shell neighbors) based on experience with other sorption systems and results from the single-shell fitting routines determined earlier.

The molecular modeling programs Cerius^2 from Accelrys, Inc. and PC Spartan Pro from Wavefunction, Inc. were used to generate visual representations of the various Hg sorption complexes proposed from interpretation of EXAFS fitting results. Energy minimization and structural optimization features of these two programs were employed to determine realistic interatomic distances and structural arrangements of the proposed Hg sorption complexes.

3. Results

3.1. Hg(II)–goethite–chloride

Macroscopic uptake results for Hg(II) sorption on goethite, γ-alumina, and bayerite as a function of [Cl^-] are shown in Fig. 3. The data show a strong decrease in Hg(II) sorption to goethite with increasing [Cl^-]; when normalized for surface area, Hg(II) surface coverages decline from 0.42 to 0.07 μmol/m^2. This phenomenon is consistent with previously reported results [4,5,20] showing that the adsorption of Hg(II) is inhibited in the presence of chloride, with the

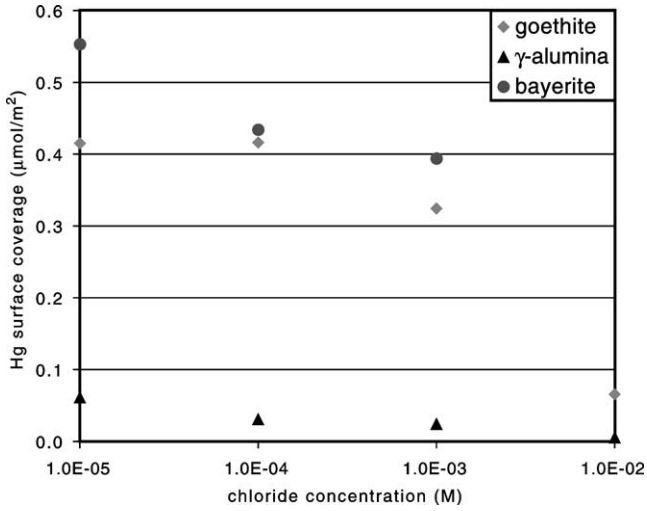

Fig. 3. Adsorption of Hg(II) by goethite, γ-alumina, and bayerite as a function of chloride concentration at pH 6. The initial concentration of Hg(II) = 0.5 mM and the solids concentration = 10 g/l. Uptake has been normalized for surface area and is expressed in units of μmol/m^2.

macroscopic adsorption edge moving to higher pH levels with increasing [Cl^-]. Formation of the stable nonsorbing $HgCl_{2(aq)}$ species in solution is commonly inferred as the reason for the reduced Hg(II) uptake. This conclusion is consistent with the speciation diagrams of Fig. 1, which show that $HgCl_{2(aq)}$ becomes the dominant aqueous Hg species at pH 6 when [Cl^-] $\geqslant 10^{-3}$ M. Additionally, the possibility of ternary surface complexation between Hg(II), chloride, and the goethite surface has been proposed by Gunneriusson and Sjoberg [5] and, using a hydrous ferric oxide (HFO) substrate, by Tiffreau et al. [33]. The former proposal has been verified by EXAFS spectroscopy [29], but there have been no spectroscopic studies of possible ternary complex formation on HFO. A generalized reaction for the formation of a ternary surface complex in the Hg(II)–goethite–chloride system was proposed by Gunneriusson and Sjoberg [5] as follows:

$$\equiv\text{FeOH} + \text{Hg}^{2+} + \text{Cl}^- \rightarrow \equiv\text{FeOHgCl} + \text{H}^+.$$

Fits of the k^3-weighted HgL_{III}-EXAFS spectra and their Fourier transforms for the Hg(II)–goethite–chloride sorption products are shown in Fig. 4. An EXAFS spectrum and Fourier transform of a Hg(II)–goethite sorption sample generated at pH 6.7 in the absence of chloride is displayed (Fig. 4e) for comparison with the spectra of the other sorption samples in which chloride was present (Figs. 4a–4d). The ligand-free sample spectra presented here and in subsequent figures were generated in a separate set of experiments from Part I of this study [18]; as such, any discrepancies in the continuity of Hg(II) uptake (e.g., uptake on the chloride-free sample is slightly less than that of the first chloride-bearing sample) are attributed to minor differences in experimental and analytical conditions between the different sets of experiments. It is more in the comparison of the raw EXAFS spectra and Fourier transforms between the ligand-

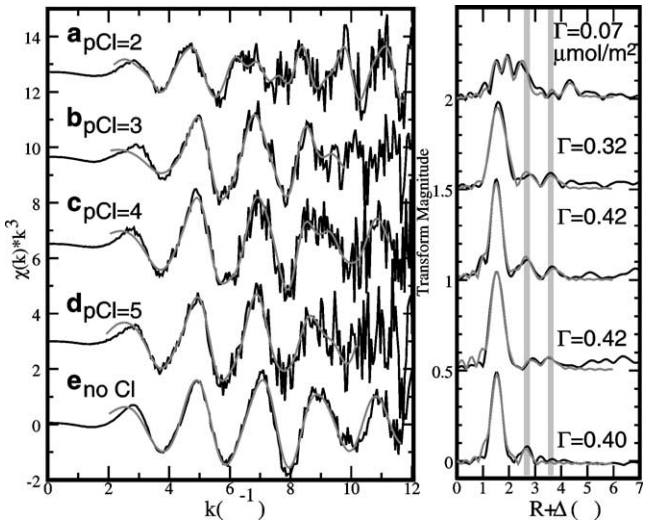

Fig. 4. Fits of the k^3-weighted EXAFS data and corresponding Fourier transforms (black, raw data; gray, fit) for Hg(II) sorbed on goethite as a function of chloride concentration at pH 6. Uptake values (Γ in μmol/m^2) are indicated to the right of the Fourier transforms. Vertical guidelines in the figure to the right show FT features due to neighboring Cl and Fe atoms at $[Cl^-] = 10^{-5}$, 10^{-4}, and 10^{-3} M.

free and ligand-bearing samples that potential changes in speciation can be discerned.

The primary structural change in the average Hg(II) sorption complex on goethite due to the presence of chloride is demonstrated by the appearance of a distant neighboring atomic shell in the Fourier transforms at ∼3.6 Å (uncorrected for phase shift). This feature indicates a change in the sorption mode from the bidentate corner-sharing arrangement of Hg(II) in the chloride-free system [34]. Results from quantitative fitting of the EXAFS spectra, shown in Table 1, identify three neighboring atomic shells beyond the initial first-neighbor O shell at 2.01–2.06 (±0.01) Å over a $[Cl^-]$ range of 10^{-5} to 10^{-3} M. These more distant shells correspond to Hg–Cl at 2.51–2.61 (±0.03) Å, Hg–Fe at 3.17–3.29 (±0.03) Å, and Hg–Fe at 3.88–4.28 (±0.03) Å. With increasing $[Cl^-]$, the coordination numbers for these neighbors approach one, likely due to decreasing proportions of outer-sphere Hg(II) complexes [35] and the increasing proportion of the ternary surface complex described in the following paragraph. The Hg–Fe pair correlations contribute to the two visible nonfirst-neighbor features in the Fourier transforms of these samples; as a result, the Hg–Cl pair correlation is considered to be less certain. However, the Hg–Cl interactions determined from EXAFS fitting match well with the proposed model as described below, so they have been included in the fitting results listed in Table 1.

Although the Hg–O distance is not sufficiently unique to distinguish between aqueous, sorbed, or precipitated Hg(II) species, the next nearest neighbors, specifically the Hg–Fe distance of 3.17–3.29 (±0.03) Å, indicate that Hg(II) continues to sorb in an inner-sphere fashion. Among the possible geometries of Hg(II) inner-sphere sorption onto the goethite surface in the presence of chloride, the one most consistent with the EXAFS fitting results is a Type A (ligand–metal-surface) ternary surface complex with the Hg–Cl species bonded in an inner-sphere monodentate mode to the $Fe(O,OH)_6$ octahedra of the (110) goethite surface, the dominant crystal face of both natural and synthetic goethite. A molecular model constructed by Spartan Pro representing this mode of sorption yields interatomic distances that agree well with those determined by EXAFS fitting (Fig. 5). Additionally, the EXAFS-derived coordination numbers correspond fairly well with those of the model, particularly for the sorption sample generated at $[Cl^-] = 10^{-3}$ M. This result confirms the hypothesis of Gunneriusson and Sjoberg [5] that Hg(II) forms a ternary surface complex with goethite in the presence of chloride and is consistent with the EXAFS study of Bargar et al. [29] that determined that Hg–chloro complexes are coordinated to goethite in a monodentate fashion through surface oxygens (i.e., Fe–O–Hg–Cl). This monodentate configuration also accounts for the variation in interatomic distances for the most distant Fe neighbor, which represents the distance between the sorbed Hg(II) ion and the center of the $Fe(O,OH)_6$ octahedron adjacent to the octahedron to which it has sorbed (Fig. 5).

At the highest $[Cl^-]$ examined (10^{-2} M), the EXAFS spectrum and Fourier transform change significantly (Fig. 4a).

Table 1
HgL_{III}-EXAFS fitting results for Hg(II)–goethite–chloride sorption samples (see Fig. 4 for EXAFS spectra and Fourier transforms), including coordination numbers (CN), interatomic distances (R), and Debye–Waller factors (σ^2)

Figure	pCl	Hg–O			Hg–Cl			Hg–Hg			Hg–Hg		
		CN	R (Å)	σ^2 (Å^2)	CN	R (Å)	σ^2 (Å^2)	CN	R (Å)	σ^2 (Å^2)	CN	R (Å)	σ^2 (Å^2)
4a	2	1.2(1)	2.09(1)	0.005[a]	1.2(1)	2.27(1)	0.005[a]	2.0(2)	2.56(1)	0.01[a]	2.5(5)	4.43(2)	0.01[a]
		Hg–O			Hg–Cl			Hg–Fe			Hg–Fe		
		CN	R (Å)	σ^2 (Å^2)	CN	R (Å)	σ^2 (Å^2)	CN	R (Å)	σ^2 (Å^2)	CN	R (Å)	σ^2 (Å^2)
4b	3	1.5(2)	2.02(1)	0.003	1.0(1)	2.52(1)	0.01[a]	1.0(1)	3.17(2)	0.01[a]	0.9(2)	4.27(2)	0.01[a]
4c	4	2.5(3)	2.01(1)	0.006	0.6(1)	2.51(2)	0.01[a]	0.8(2)	3.20(2)	0.01[a]	1.0(3)	4.28(3)	0.01[a]
4d	5	2.7(2)	2.06(1)	0.007	0.4(2)	2.61(3)	0.01[a]	0.5(2)	3.29(3)	0.01[a]	0.8(2)	3.88(2)	0.01[a]
4e	None	2.4(1)	2.02(1)	0.005				0.6(1)	3.19(1)	0.01[a]			

Standard deviations at a 95% confidence level (±2σ) are listed in parentheses.
[a] Value fixed in least-squares refinement.

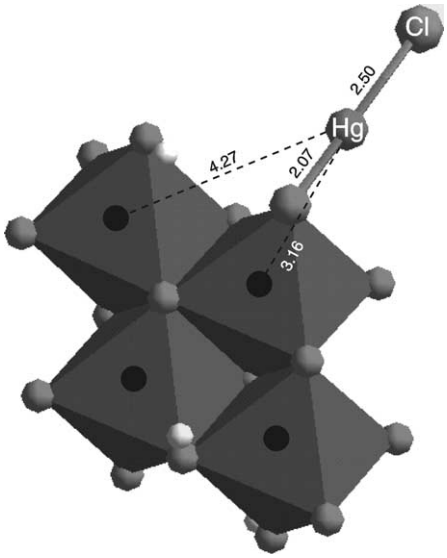

Fig. 5. Proposed Hg(II) bonding configuration on goethite in the presence of chloride, with Hg(II) sorbing as a Type A ternary surface complex bonded monodentate with chloride.

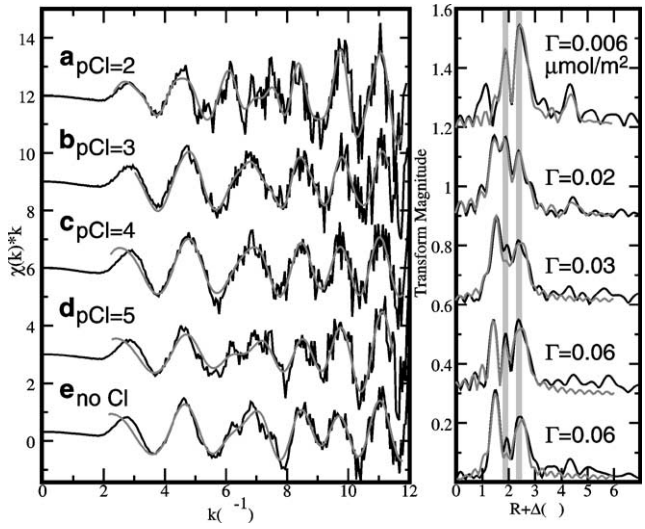

Fig. 6. Fits of the k^3-weighted EXAFS data and corresponding Fourier transforms (black, raw data; gray, fit) for Hg(II) sorbed on γ-alumina as a function of chloride concentration at pH 6. Uptake values (Γ in μmol/m^2) are indicated to the right of the Fourier transforms. Vertical guidelines in the figure to the right show FT features due to neighboring O and Hg atoms at $[Cl^-] = 10^{-5}$, 10^{-4}, and 10^{-3} M.

Fitting of this spectrum yields a Hg–O distance of 2.09 (±0.01) Å, a Hg–Cl distance of 2.27 (±0.01) Å, and Hg–Hg distances of 2.56 (±0.01) and 4.43 (±0.02) Å. The Hg–O distance is similar to that of the previous samples; however, as discussed in Part I [18], a Hg–Hg distance of ∼2.55 Å is strongly suggestive of dimeric Hg(I) species and indicates that Hg(II) has been subjected to beam-induced photoreduction during EXAFS data collection, a phenomenon which has also been observed for $CuCl_2$ [36] and $AuCl_3$ [37] aqueous complexes. Hg(II) reduction to Hg(I) is expected to be more prominent when there is a high proportion of Hg(II) in solution (i.e., in systems with low adsorption), such as that observed at the highest [Cl$^-$]. The EXAFS fitting results are consistent with the Hg(I) compound calomel, $Hg_2Cl_{2(s)}$, which features Hg–Cl distances of 2.30 Å and Hg–Hg distances of 2.59 Å [38], and indicate that Hg has precipitated as calomel and/or is present as aqueous Hg_2Cl_2 species.

3.2. Hg(II)–γ-alumina–chloride

Macroscopic uptake results for Hg(II) on γ-alumina in the presence of chloride (Fig. 3) show a drop in Hg(II) sorption with increasing [Cl$^-$], similar to the trend observed for the other substrates. Hg surface coverages decline from 0.06 to 0.006 μmol/m^2 over the range of [Cl$^-$] examined. Throughout this series of samples, the degree of Hg(II) sorption was lower on γ-alumina than on either goethite or bayerite, as previously observed in the ligand-free system [18].

Fits to the experimental k^3-weighted HgL_{III}-EXAFS spectra and their Fourier transforms for the Hg(II)–γ-alumina–chloride sorption products are shown in Fig. 6, with the spectrum of a chloride-free sample generated in Part I at pH 6 for comparison (Fig. 6e). Although no particular visible trend in the Fourier transforms is apparent with increasing [Cl$^-$], the EXAFS fitting results (Table 2) are very similar from 10^{-5} to 10^{-3} M [Cl$^-$], yielding O neighbors at 2.02–2.04 (±0.02) Å and 2.20–2.22 (±0.01) Å, and one Hg neighbor at 2.56–2.58 (±0.01) Å. These results are comparable to those for the ligand-free sample (Fig. 6e) [18], suggesting that the mode of Hg(II) sorption onto γ-alumina in the presence of chloride is largely similar to that in the absence of chloride. At 10^{-3} M [Cl$^-$] there is the appearance of a Hg–Hg neighbor at 4.53 Å, which becomes even more prominent at 10^{-2} M [Cl$^-$] and is thought, as seen earlier (Fig. 4a), to indicate the beginnings of $Hg_2Cl_{2(s)}$ precipitation.

As discussed in Part I [18], γ-alumina undergoes hydration in aqueous solution, causing the $Al(O,OH)_4$ tetrahedra at the γ-alumina surface to convert to $Al(O,OH)_6$ octahedra [39–41]. Over time periods in excess of one month, this eventually results in a surface conversion to bayerite as observed by Dyer et al. [42] and Laiti et al. [43]. Beam-induced photoreduction of Hg(II) to Hg(I) was observed throughout this system, likely due to the high proportion of Hg(II) in solution resulting from low total uptake to the γ-alumina substrate. The subsequent sorption of $Hg_2(OH)_{2(aq)}$ to the hydrated γ-alumina surface was described in Part I as a combination of monodentate and bidentate corner-sharing sorption complexes, of which certain complexes are bonded to Al-octahedra that bridge the octahedral rows of the hydrated γ-alumina structure (see Fig. 9 in [18]). The spectral evidence indicates that even in the presence of chloride, the dominant modes of Hg sorption to γ-alumina are similar to those in the absence of chloride, so that the observed reduction in total Hg uptake is due primarily to the formation of stable aqueous $HgCl_{2(aq)}$ or $Hg_2Cl_{2(aq)}$ species. The absence of identifiable chloride neighbors in these spectra also in-

Table 2
HgL_{III}-EXAFS fitting results for Hg(II)–γ-alumina–chloride sorption samples (see Fig. 6 for EXAFS spectra and Fourier transforms), including coordination numbers (CN), interatomic distances (R), and Debye–Waller factors (σ^2)

Figure	pCl	Hg–Cl			Hg–Hg			Hg–Hg		
		CN	R (Å)	σ^2 (Å^2)	CN	R (Å)	σ^2 (Å^2)	CN	R (Å)	σ^2 (Å^2)
6a	2	2.8(5)	2.28(1)	0.016	1.4(1)	2.57(1)	0.005[a]	2.6(6)	4.47(2)	0.01[a]
		Hg–O			Hg–O			Hg–Hg		
		CN	R (Å)	σ^2 (Å^2)	CN	R (Å)	σ^2 (Å^2)	CN	R (Å)	σ^2 (Å^2)
6b	3	1.1(1)	2.04(1)	0.005[a]	1.7(1)	2.21(1)	0.005[a]	0.8(1)	2.56(1)	0.005[a]
6c	4	1.3(1)	2.04(1)	0.005[a]	1.5(1)	2.21(1)	0.005[a]	0.9(1)	2.58(1)	0.005[a]
6d	5	1.1(1)	2.02(1)	0.005[a]	1.5(1)	2.22(1)	0.005[a]	0.9(1)	2.56(1)	0.005[a]
6e	None	1.4(1)	2.04(1)	0.005[a]	1.3(1)	2.22(1)	0.005[a]	0.8(1)	2.56(1)	0.005[a]

Standard deviations at a 95% confidence level ($\pm 2\sigma$) are listed in parentheses.
[a] Value fixed in least-squares refinement.

dicates that ternary surface complexation is not a dominant process occurring in this system, or that ternary surface complexes may be present in minor proportions which could not be easily observed with EXAFS spectroscopy.

At 10^{-2} M [Cl^-], however, changes in both the EXAFS spectrum and Fourier transform relative to those of the lower [Cl^-] samples suggest differences in both the speciation and the mode of sorption for Hg. EXAFS fitting yields structural information similar to that of the Hg-goethite sorption sample generated at 10^{-2} M [Cl^-] (Table 1), with a Hg–Cl distance of 2.28 ($\pm$0.01) Å and Hg–Hg distances of 2.57 ($\pm$0.01) and 4.47 ($\pm$0.02) Å. These results also indicate that the low uptake of Hg(II), resulting in elevated proportions of aqueous Hg(II), has resulted in beam reduction of Hg(II) to Hg(I) and subsequent precipitation of $Hg_2Cl_{2(s)}$/formation of $Hg_2Cl_{2(aq)}$ complexes.

3.3. Hg(II)–bayerite–chloride

Macroscopic uptake results for Hg(II) sorption on bayerite in the presence of chloride (Fig. 3) show that, as with goethite and γ-alumina, uptake of Hg(II) is substantially reduced with increasing chloride. Surface coverages decrease from 0.55 to 0.39 µmol/m^2 over a range of 10^{-5} to 10^{-3} M [Cl^-]. Over the range of [Cl^-] examined, the effects of chloride on the degree of Hg(II) sorption to bayerite are generally comparable with those observed in the Hg(II)–goethite–chloride system. This is in accordance with the earlier sorption study [18] which showed that bayerite and goethite have similar uptake trends as a function of pH.

EXAFS spectra and Fourier transforms for the Hg(II)–bayerite–chloride system are shown in Fig. 7, with fitting results in Table 3. The Fourier transforms of sample spectra in the presence of 10^{-5} and 10^{-4} M chloride (Figs. 7c and 7b) resemble those of the chloride-free spectrum generated in Part I [18] (Fig. 7d), indicating that the modes of sorption are similar. As mentioned earlier, the apparent lower uptake of the chloride-free sample relative to the others is likely due to slightly different experimental conditions and should not be construed as a deviation of the trend of decreasing Hg(II) uptake with increasing chloride. Fits of these two EXAFS spectra (Table 3) result in an Hg–O distance of 2.06–2.07 ($\pm$0.01) Å and Hg–Al distances of 3.03–3.04 ($\pm$0.02) and 3.33–3.42 ($\pm$0.04) Å, which are similar to the fitting results of the ligand-free sorption sample. Hg(II) was observed to sorb to bayerite in the absence of chloride dominantly as monodentate, bidentate corner-sharing, and bidentate edge-sharing complexes [18]. The similarity in EXAFS fitting results between the chloride-bearing and chloride-free sorption experiments suggests that the same modes of Hg(II) sorption are dominant at [Cl^-] = 10^{-5} and 10^{-4} M and that aqueous $HgCl_2$ species formation causes the reduced Hg(II) uptake. As with the γ-alumina system, the absence of identifiable chloride neighbors also indicates that ternary surface complexation is not a significant mode of Hg(II) uptake at these chloride concentrations.

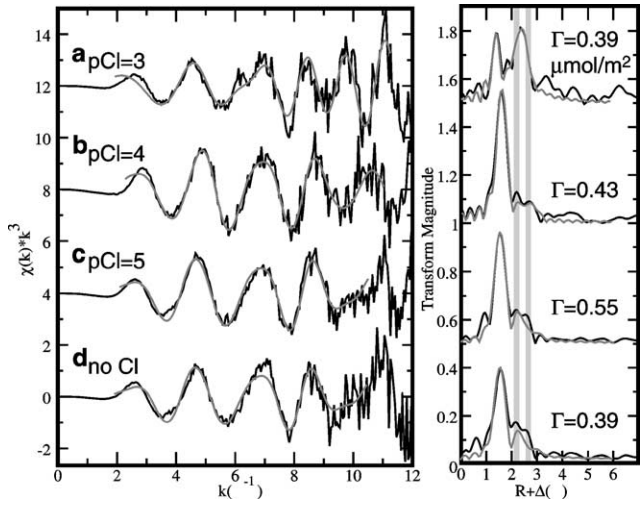

Fig. 7. Fits of the k^3-weighted EXAFS data and corresponding Fourier transforms (black, raw data; gray, fit) for Hg(II) sorbed on bayerite as a function of chloride concentration at pH 6. Uptake values (Γ in µmol/m^2) are indicated to the right of the Fourier transforms. Vertical guidelines in the figure to the right show FT features due to second-neighbor Al atoms at [Cl^-] = 10^{-5} and 10^{-4} M.

At 10^{-3} M [Cl^-], there is a significant change in both the EXAFS spectrum and the Fourier transform relative to the

Table 3
HgL_{III}-EXAFS fitting results for Hg(II)–bayerite–chloride sorption samples (see Fig. 7 for EXAFS spectra and Fourier transforms), including coordination numbers (CN), interatomic distances (R), and Debye–Waller factors (σ^2)

Figure	pCl	Hg–O			Hg–O			Hg–Hg		
		CN	R (Å)	σ^2 (Å^2)	CN	R (Å)	σ^2 (Å^2)	CN	R (Å)	σ^2 (Å^2)
7a	3	1.4(1)	2.02(1)	0.005[a]	1.7(2)	2.20(1)	0.005[a]	1.4(1)	2.54(1)	0.005[a]
		Hg–O			Hg–Al			Hg–Al		
		CN	R (Å)	σ^2 (Å^2)	CN	R (Å)	σ^2 (Å^2)	CN	R (Å)	σ^2 (Å^2)
7b	4	2.3(2)	2.07(1)	0.006	0.9(2)	3.03(2)	0.01[a]	0.6(3)	3.42(4)	0.01[a]
7c	5	2.3(2)	2.06(1)	0.007	1.6(2)	3.04(1)	0.01[a]	1.0(3)	3.33(2)	0.01[a]
7d	None	1.9(2)	2.07(1)	0.006	1.6(3)	3.07(1)	0.01[a]	1.1(4)	3.35(2)	0.01[a]

Standard deviations at a 95% confidence level ($\pm 2\sigma$) are listed in parentheses.
[a] Value fixed in least-squares refinement.

lower [Cl^-] samples (Fig. 7a). Fitting of the EXAFS spectral data and visual comparison to the spectra in Fig. 6 indicate that the mode of Hg(II) sorption in this system is similar to that of the Hg(II)–γ-alumina system and the Hg(II)–γ-alumina–chloride system as described earlier. Specifically, the EXAFS fitting results as summarized in Table 3 identify Hg–O at 2.02 (±0.01) Å, Hg–O at 2.20 (±0.01) Å, and Hg–Hg at 2.54 (±0.01) Å, comparable to the fitting results in Table 2. The close Hg–Hg distance again indicates that Hg(I) dimers have been produced through beam reduction of unsorbed aqueous Hg(II) at elevated chloride concentrations, while the intermediate Hg–O distance of 2.20 (±0.01) Å can be correlated with sorption of the $Hg_2(OH)_2$ species in monodentate or bidentate corner-sharing modes to Al octahedra as discussed earlier [18].

3.4. Hg(II)–goethite–sulfate

Figure 8 shows the uptake of Hg(II) on goethite, γ-alumina, and bayerite as a function of sulfate concentration, [SO_4^{2-}]. Again, the degree of uptake has been normalized for surface area and is shown in units of µmol/m^2. A wider range of [SO_4^{2-}] (10^{-5} to ∼1 M) was investigated here than of chloride due to the enhancement of Hg(II) sorption by sulfate, which makes EXAFS analysis more feasible at higher ligand concentrations. Hg(II) sorption density on goethite increases with increasing [SO_4^{2-}] from 0.39 to 0.45 µmol/m^2 over the range of [SO_4^{2-}] examined. An earlier study of the sorption of Pb(II) to goethite shows a similar effect, with Pb uptake enhanced by at least 30% in the presence of 3.16 mM sulfate [10]. From a macroscopic viewpoint, this trend in uptake with increasing [SO_4^{2-}] suggests inner-sphere sorption of Hg(II), as outer-sphere sorption would be expected to yield the opposite trend with increasing ionic strength.

The EXAFS spectra and Fourier transforms of the sorption products over the [SO_4^{2-}] range of 10^{-5} to 10^{-1} M (Figs. 9b–9f) are comparable to those of the ligand-free sorption sample generated in Part I (Fig. 9g). Fitting of these spectra yields O and Fe neighbors at 2.03–2.05 (±0.01) and 3.20–3.26 (±0.02) Å, respectively (Table 4). These results

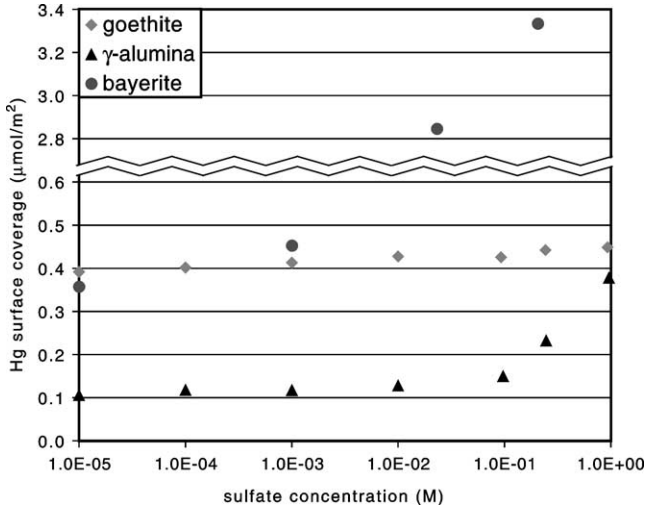

Fig. 8. Adsorption of Hg(II) by goethite, γ-alumina, and bayerite as a function of sulfate concentration at pH 6. The initial concentration of Hg(II) = 0.5 mM and the solids concentration = 10 g/l (5 g/l for the γ-alumina samples). Uptake has been normalized for surface area and is expressed in units of µmol/m^2.

indicate that the mode of Hg(II) sorption is unchanged from that of the sulfate-free system, in which Hg(II) forms bidentate inner-sphere sorption complexes in a corner-sharing configuration to the $Fe(O,OH)_6$ octahedra of the goethite surface [18]. Aqueous speciation diagrams of these systems (Fig. 2) show that Hg–sulfate aqueous complexes are not present in significant proportions at these concentrations, so ternary surface complexation is not likely. The enhanced affinity of Hg(II) to goethite in the presence of sulfate is hypothesized to result from sulfate accumulation or sorption at the goethite surface, thereby reducing the electrostatic repulsion that Hg(II) encounters when sorbing to the positively charged goethite surface below its pH_{pzc} (7.8) [44]. The ATR-FTIR analysis of Ostergren et al. [10] showed that sulfate sorbs to goethite as a combination of monodentate and nonprotonated outer-sphere complexes at neutral pH, which supports the proposed explanation for increased Hg(II) sorption with increasing [SO_4^{2-}].

At the highest [SO_4^{2-}] (0.93 M), there is a noticeable shift in the second-neighbor Fe distance from 3.26 to 3.70 Å

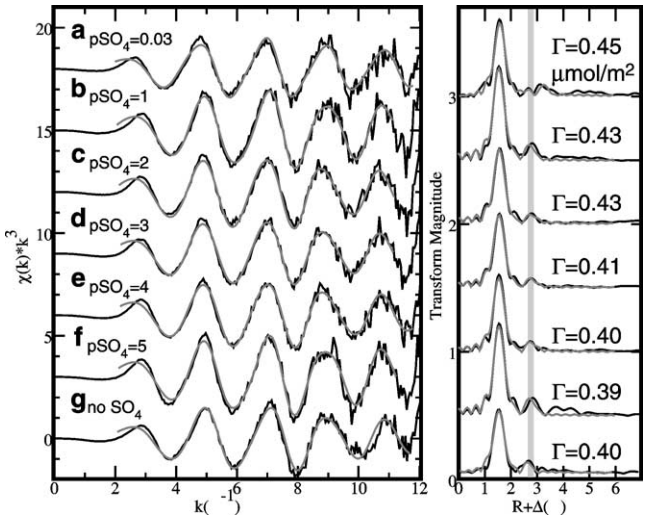

Fig. 9. Fits of the k^3-weighted EXAFS data and corresponding Fourier transforms (black, raw data; gray, fit) for Hg(II) sorbed on goethite as a function of sulfate concentration at pH 6. Uptake values (Γ in μmol/m^2) are indicated to the right of the Fourier transforms. The vertical guideline in the figure to the right shows the shift in the second-neighbor Fe distance at the highest sulfate concentration.

Table 4
HgL_{III}-EXAFS fitting results for Hg(II)–goethite–sulfate sorption samples (see Fig. 9 for EXAFS spectra and Fourier transforms), including coordination numbers (CN), interatomic distances (R), and Debye–Waller factors (σ^2)

Figure	pSO$_4$	Hg–O			Hg–Fe		
		CN	R (Å)	σ^2 (Å^2)	CN	R (Å)	σ^2 (Å^2)
9a	0.03	2.5(1)	2.04(1)	0.006	0.7(1)	3.70(1)	0.01[a]
9b	1	2.5(1)	2.03(1)	0.004	0.7(1)	3.26(1)	0.01[a]
9c	2	2.4(1)	2.05(1)	0.005	0.5(1)	3.22(1)	0.01[a]
9d	3	2.4(1)	2.04(1)	0.005	0.4(1)	3.24(1)	0.01[a]
9e	4	2.5(1)	2.03(1)	0.005	0.5(1)	3.20(1)	0.01[a]
9f	5	2.6(1)	2.03(1)	0.004	0.8(1)	3.25(1)	0.01[a]
9g	None	2.5(1)	2.04(1)	0.006	0.4(1)	3.24(2)	0.01[a]

Standard deviations at a 95% confidence level ($\pm 2\sigma$) are listed in parentheses.
[a] Value fixed in least-squares refinement.

(Fig. 9a, Table 4). This increase of 0.44 Å implies a change in the sorption mode of Hg(II) at the goethite surface. Although aqueous Hg–sulfate complexes are still not significant, the additional expected sorption of sulfate at the goethite surface at 0.93 M [SO_4^{2-}] increases the possibility of Hg(II) ternary surface complexation. Figure 10 shows a proposed Type A ternary complex bound to the surface through Hg in a monodentate mode with sulfate bound to the Hg in a monodentate fashion, which is consistent with the EXAFS fitting results for sample 9a. At high [SO_4^{2-}] approaching 1 M, it may be possible for these types of Hg(II) ternary surface complexes to form. However, because such concentrations are rare in natural environments, it is more probable that Hg(II) uptake on goethite is enhanced primarily by surface charge reduction through direct sulfate sorption to the goethite surface, resulting in little change in the Hg(II) sorption mode from the sulfate-free system as indicated by the EXAFS fitting results.

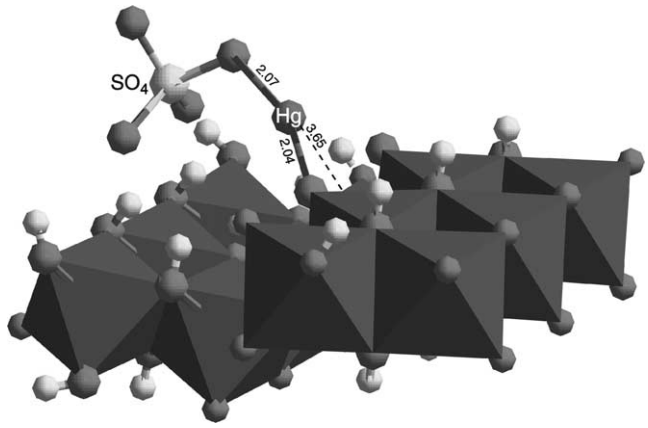

Fig. 10. Proposed Hg(II) bonding configuration on goethite in the presence of sulfate, with Hg(II) bound to the goethite surface and with sulfate bound to the Hg(II) in a monodentate fashion.

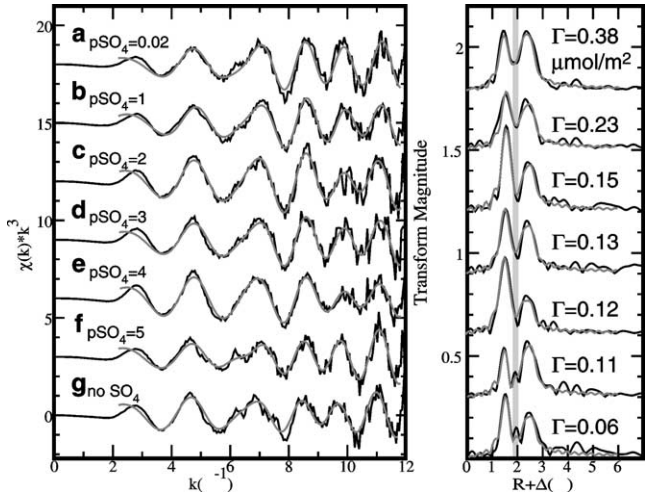

Fig. 11. Fits of the k^3-weighted EXAFS data and corresponding Fourier transforms (black, raw data; gray, fit) for Hg(II) sorbed on γ-alumina as a function of sulfate concentration at pH 6. Uptake values (Γ in μmol/m^2) are indicated to the right of the Fourier transforms. The vertical guideline in the figure to the right shows the diminution of the FT feature that is related to the possible suppression of a surface conversion from γ-alumina to a bayerite-like phase.

3.5. Hg(II)–γ-alumina–sulfate

Macroscopic uptake measurements of Hg(II) on γ-alumina as a function of [SO_4^{2-}] (Fig. 8) also show an increase in Hg(II) uptake with increasing [SO_4^{2-}] sulfate concentration. Mercury uptake rose from 0.11 to 0.38 μmol/m^2 over the sulfate concentration range investigated. Because of the higher amounts of sorbed Hg(II) on the substrate, spectral quality is improved relative to the EXAFS spectra of sorption samples containing chloride. As a result, a progressive trend is more easily observed in both the EXAFS spectra and the Fourier transforms (Fig. 11). As [SO_4^{2-}] increases, the

Table 5
HgL_{III}-EXAFS fitting results for Hg(II)–γ-alumina–sulfate sorption samples (see Fig. 11 for EXAFS spectra and Fourier transforms), including coordination numbers (CN), interatomic distances (R), and Debye–Waller factors (σ^2)

Figure	pSO_4	Hg–O			Hg–O			Hg–Hg		
		CN	R (Å)	σ^2 (Å^2)	CN	R (Å)	σ^2 (Å^2)	CN	R (Å)	σ^2 (Å^2)
11a	0.02	1.1(1)	1.99(1)	0.005[a]	1.1(1)	2.14(1)	0.005[a]	1.2(1)	2.52(1)	0.005[a]
11b	1	1.0(1)	2.05(1)	0.005[a]	0.7(1)	2.17(1)	0.005[a]	0.9(1)	2.54(1)	0.005[a]
11c	2	1.8(1)	2.06(1)	0.005[a]	0.7(1)	2.22(2)	0.005[a]	1.0(1)	2.54(1)	0.005[a]
11d	3	1.3(1)	2.04(1)	0.005[a]	0.9(1)	2.19(1)	0.005[a]	1.0(1)	2.54(1)	0.005[a]
11e	4	1.5(1)	2.04(1)	0.005[a]	1.1(1)	2.17(1)	0.005[a]	0.7(1)	2.54(1)	0.005[a]
11f	5	1.1(1)	2.03(1)	0.005[a]	1.2(1)	2.22(1)	0.005[a]	1.0(1)	2.55(1)	0.005[a]
11g	None	1.4(1)	2.04(1)	0.005[a]	1.3(1)	2.22(1)	0.005[a]	0.8(1)	2.56(1)	0.005[a]

Standard deviations at a 95% confidence level ($\pm 2\sigma$) are listed in parentheses.
[a] Value fixed in least-squares refinement.

shoulder in the EXAFS spectra at $k = \sim 6.3$ Å^{-1} becomes less pronounced, as does the central peak in the Fourier transform. As discussed earlier and in Part I [18], these features are indicative of the sorption of Hg(I) dimers onto the Al-octahedra that form through hydration and bridge the Al-octahedral rows of the hydrated γ-alumina structure, yielding a bayerite-like structure. The gradual diminution of these features with increasing $[SO_4^{2-}]$ implies that this mode of sorption becomes rarer as $[SO_4^{2-}]$ increases. EXAFS fitting results are given in Table 5 and yield structural information similar to that for the sulfate-free system, with O neighbors at 1.99–2.06 (± 0.01) and 2.14–2.22 (± 0.02) Å and an Hg neighbor at 2.52–2.56 (± 0.01) Å (the Hg–Hg distance again indicates beam-induced reduction of Hg(II) to Hg(I) dimers). Results from Table 5 also show that the coordination number of the Hg–O pair correlation at 2.20 (± 0.02) Å decreases (from 1.2 to 0.7) as $[SO_4^{2-}]$ increases from 10^{-5} to 10^{-1} M, consistent with the diminution of this central peak feature in the Fourier transforms. Otherwise, Hg appears to sorb onto γ-alumina in a manner similar to that observed in both sulfate-bearing and sulfate-free systems (i.e., as Hg(I) dimers sorbing in both monodentate and bidentate corner-sharing modes).

These results suggest that increasing $[SO_4^{2-}]$ suppresses the surface conversion of γ-alumina to the bayerite-like structure observed with hydration [18]. This may occur as a result of increasing sulfate sorption onto γ-alumina with increasing $[SO_4^{2-}]$, limiting the dissolution of γ-alumina and the formation/reordering of the bayerite-like phase at the substrate surface. As with the Hg(II)–goethite–sulfate system, the additional reduction of positive surface charge resulting from sulfate sorption to the substrate likely allows the enhanced sorption of Hg(I) on γ-alumina relative to the substrate-free system. Prior studies reporting the non-specific adsorption of sulfate to the γ-alumina surface [45,46] support this explanation for enhanced Hg(I) uptake with increasing $[SO_4^{2-}]$. No evidence of ternary surface complexation is observed from EXAFS fitting, indicating that the enhanced Hg(I) sorption is promoted primarily by sulfate sorption on γ-alumina and charge lowering at the substrate surface.

3.6. Hg(II)–bayerite–sulfate

Macroscopic uptake results of Hg(II) onto bayerite (Fig. 8) show enhanced Hg(II) uptake with increasing $[SO_4^{2-}]$, rising from 0.36 to 3.33 μmol/m^2 over the range of $[SO_4^{2-}]$ investigated. This change represents nearly an order of magnitude increase in Hg(II) uptake and is the most significant enhancement in Hg(II) uptake caused by sulfate observed in this study. Additionally, surface coverages at sulfate concentrations of 10^{-1} and 0.89 M exceed 1 μmol/m^2, raising the possibility of Hg(II) precipitation at the bayerite surface. Identical Hg(II) and sulfate concentrations in the Hg–goethite–sulfate and Hg–γ-alumina–sulfate systems did not produce similar results, indicating that the precipitation is influenced by the bayerite surface and does not occur in solution.

The EXAFS spectra and nearest neighbor features in the Fourier transforms of the sorption samples at 10^{-5} and

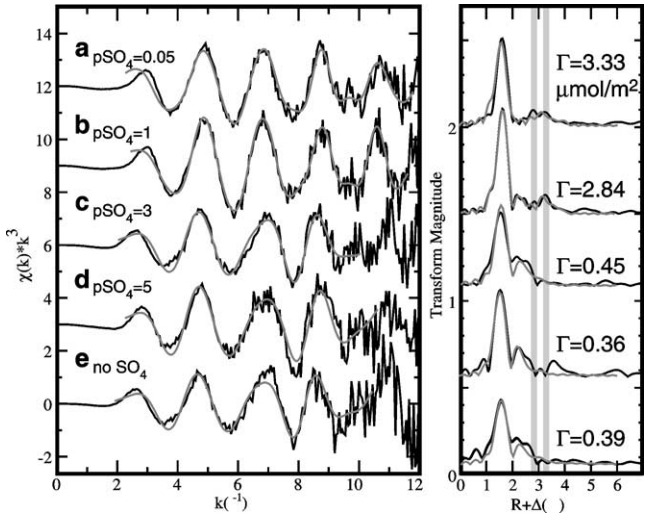

Fig. 12. Fits of the k^3-weighted EXAFS data and corresponding Fourier transforms (black, raw data; gray, fit) for Hg(II) sorbed on bayerite as a function of sulfate concentration at pH 6. Uptake values (Γ in μmol/m^2) are indicated to the right of the Fourier transforms. The vertical guidelines in the figure to the right show the changes in the Fourier transforms corresponding to the possible precipitation of $HgO_{(s)}$ at high $[SO_4^{2-}]$.

Table 6
HgL_{III}-EXAFS fitting results for Hg(II)–bayerite–sulfate sorption samples (see Fig. 12 for EXAFS spectra and Fourier transforms), including coordination numbers (CN), interatomic distances (R), and Debye–Waller factors (σ^2)

Figure	pSO_4	Hg–O			Hg–Hg/Hg–Al			Hg–Hg/Hg–Al			Notes
		CN	R (Å)	σ^2 (Å^2)	CN	R (Å)	σ^2 (Å^2)	CN	R (Å)	σ^2 (Å^2)	
12a	0.05	2.3(1)	2.06(1)	0.006	1.1(2)	3.20(1)	0.01[a]	0.9(3)	3.89(2)	0.01[a]	O/Hg/Hg
12b	1	2.5(1)	2.07(1)	0.005	1.1(2)	2.89(1)	0.01[a]	1.4(3)	3.15(2)	0.01[a]	O/Al/Al
					1.5(3)	3.22(1)	0.01[a]	1.1(3)	3.85(2)	0.01[a]	Hg/Hg
12c	3	2.0(2)	2.06(1)	0.006	1.6(2)	3.06(1)	0.01[a]	1.0(3)	3.36(2)	0.01[a]	O/Al/Al
12d	5	2.1(2)	2.04(1)	0.006	2.0(3)	3.01(1)	0.01[a]	1.2(4)	3.28(2)	0.01[a]	O/Al/Al
12e	None	1.9(2)	2.07(1)	0.006	1.6(3)	3.07(1)	0.01[a]	1.1(4)	3.35(2)	0.01[a]	O/Al/Al

Standard deviations at a 95% confidence level ($\pm 2\sigma$) are listed in parentheses. The rightmost column gives the elemental nature of the successive (i.e., second and third) atomic shells around Hg according to the fitting results.
[a] Value fixed in least-squares refinement.

10^{-3} M [SO_4^{2-}] (Figs. 12d and 12c) are similar to those of the ligand-free sample generated in Part I (Fig. 12e), indicating that the modes of sorption in the sulfate-bearing system and sulfate-free system are similar. This is supported by the fitting results (Table 6), which show two O neighbors at 2.04–2.06 (± 0.01) Å and Al neighbors at 3.01–3.06 (± 0.01) and 3.28–3.36 (± 0.02) Å, similar to the fitting results for sample 12e. Therefore, Hg(II) likely sorbs dominantly in monodentate and bidentate corner- and edge-sharing modes on bayerite at these sulfate concentrations, as was found for the ligand-free system [18]. At 10^{-1} and 0.89 M [SO_4^{2-}] (Figs. 12b and 12a), however, two more distant features appear in the Fourier transforms indicating a different mode of Hg(II) association with the bayerite surface. Fitting of these spectra identifies the two furthest neighbors as Hg at distances of 3.20–3.22 (± 0.01) and 3.85–3.89 (± 0.02) Å, respectively. These results are approximately consistent with the coordination of Hg in orthorhombic $HgO_{(s)}$, which contains 2 O neighbors at 2.03 Å and Hg neighbors at 3.30 and 3.73 Å [47]. Together with the macroscopic uptake data showing surface coverages exceeding 1 μmol/m^2 at these elevated sulfate concentrations, the EXAFS data suggest that $HgO_{(s)}$ precipitation at the surface has occurred. This may be a result of greatly enhanced Hg(II) sorption at high [SO_4^{2-}] to the point of reaching supersaturation with respect to $HgO_{(s)}$ in the very localized region directly at the surface, although this cannot be experimentally verified. As discussed earlier, this enhanced uptake is attributed to the reduction of positive surface charge through the sorption of sulfate to bayerite.

4. Conclusions

Chloride and sulfate ligands have pronounced effects on Hg(II) sorption, with chloride resulting in reduced Hg(II) uptake on goethite, γ-alumina, and bayerite and with sulfate resulting in enhanced Hg(II) uptake on the same sorbents under similar conditions. Aqueous speciation diagrams, macroscopic uptake measurements, and EXAFS spectroscopic analysis of sorption products have been used to identify the molecular-level phenomena that cause these effects. In the case of chloride, the stability of the nonsorbing $HgCl_2$ aqueous species, which are the dominant Hg phase at [Cl^-] $\geqslant 10^{-3}$ M and pH 6, limits the amount of Hg(II) sorption on these substrates. At these higher chloride levels, the large proportion of unsorbed aqueous Hg(II) resulting from the presence of chloride also seems to facilitate X-ray beam-induced photoreduction of Hg(II) to Hg(I) and the formation of $Hg_2Cl_{2(s)}$ or $Hg_2Cl_{2(aq)}$ species. Sulfate, in contrast, complexes much less readily with Hg(II) in solution and is more likely to sorb to the substrate surface, thereby lowering the electrostatic repulsion that Hg(II) must overcome to sorb to the positively charged surfaces at neutral pH and resulting in the enhanced Hg(II) uptake observed macroscopically.

Ternary surface complexation may occur in the presence of chloride or sulfate, particularly at high ligand concentrations as observed with the Hg(II)–goethite–chloride and Hg(II)–goethite–sulfate systems. In some cases, surface precipitation may take place, as inferred in the Hg(II)–bayerite–sulfate system. Generally, however, the modes of Hg(II) sorption in the presence of these ligands are similar to those of the corresponding ligand-free systems, indicating that stable aqueous complex formation and electrostatic surface charge reduction are primarily responsible for the observed effects of chloride and sulfate, respectively, on Hg(II) sorption.

Molecular-scale studies of Hg(II) uptake to mineral surfaces in model systems provide an important basis for identifying sorption processes involving Hg(II) in contaminated natural environments. The inclusion of complexing ligands in Hg(II) sorption studies moves one step beyond binary contaminant–substrate model systems and demonstrates the potential direct and indirect impacts of ligands on Hg(II) uptake. Spectroscopic studies of the sorption products generated in the presence of chloride and sulfate allow identification of possible changes in sorption mode at the molecular scale. Such information adds to our understanding of the stability of the sorbed Hg(II) complex under more complex conditions, which can impact its potential for sequestration, desorption, and future bioavailability in natural aqueous systems.

Acknowledgments

We thank the staff of the Stanford Synchrotron Radiation Laboratory (SSRL), particularly John Bargar and Joe Rogers, for their assistance during EXAFS data collection. SSRL is supported by the Department of Energy (Office of Basic Energy Sciences and Office of Health and Environmental Sciences) and the National Institutes of Health. Guangchou Li (Stanford University) provided critical support in conducting all ICP analyses. Jeff Catalano (Stanford University) assisted with aqueous speciation diagram modeling using Geochemist's Workbench. We also thank two anonymous reviewers whose comments greatly improved the manuscript. This study was supported by the U.S. Environmental Protection Agency Science To Achieve Results program (US EPA-STAR Program Grant EPA-R827634-01-1) and the U.S. Geological Survey, Geologic Division.

References

[1] E. Schuster, Water Air Soil Pollut. 45 (1991) 667.
[2] W. Stumm, J.J. Morgan, Aquatic Chemistry, Wiley, New York, 1996.
[3] J.R. Bargar, G.E. Brown Jr., G.A. Parks, Geochim. Cosmochim. Acta 62 (1998) 193.
[4] N.J. Barrow, V.C. Cox, J. Soil Sci. 43 (1992) 295.
[5] L. Gunneriusson, S. Sjoberg, J. Colloid Interface Sci. 156 (1993) 121, doi:10.1006/jcis.1993.1090.
[6] M.G. MacNaughton, R.O. James, J. Colloid Interface Sci. 47 (1974) 431.
[7] B.C. Bostick, S. Fendorf, M.O. Barnett, P.M. Jardine, S.C. Brooks, Soil Sci. Soc. Am. J. 66 (2002) 99.
[8] S.F. Cheah, G.E. Brown Jr., G.A. Parks, Geochim. Cosmochim. Acta 63 (1999) 3229.
[9] J.J. Lenhart, J.R. Bargar, J.A. Davis, J. Colloid Interface Sci. 234 (2001) 448, doi:10.1006/jcis.2000.7345.
[10] J.D. Ostergren, G.E. Brown Jr., G.A. Parks, P. Persson, J. Colloid Interface Sci. 225 (2000) 483, doi:10.1006/jcis.1999.6702.
[11] P.W. Schindler, in: M.F. Hochella Jr., A.F. White (Eds.), Co-adsorption of Metal Ions and Organic Ligands: Formation of Ternary Surface Complexes, Mineralogical Society of America, Blacksburg, VA, 1990, p. 282.
[12] M.M. Benjamin, J.O. Leckie, Environ. Sci. Technol. 16 (1982) 162.
[13] T.L. Theis, M.J. West, Environ. Technol. Lett. 7 (1986) 309.
[14] U. Hoins, L. Charlet, H. Sticher, Water Air Soil Pollut. 68 (1993) 241.
[15] J.D. Ostergren, T.P. Trainor, J.R. Bargar, G.E. Brown Jr., G.A. Parks, J. Colloid Interface Sci. 225 (2000) 466, doi:10.1006/jcis.1999.6701.
[16] C.R. Collins, K.V. Ragnarsdottir, D.M. Sherman, Geochim. Cosmochim. Acta 63 (1999) 2989.
[17] M.A. Ali, D.A. Dzombak, Geochim. Cosmochim. Acta 60 (1996) 291.
[18] C.S. Kim, J.J. Rytuba, G.E. Brown Jr., J. Colloid Interface Sci., in press.
[19] D.E. White, C.E. Roberson, in: A.E.J. Engel, H.L. James, B.F. Leonard (Eds.), Sulphur Bank, California: A Major Hot-Spring Quicksilver Deposit, Geological Society of America, 1962, p. 397.
[20] E.A. Forbes, A.M. Posner, J.P. Quirk, J. Colloid Interface Sci. 49 (1974) 403.
[21] H.C. Hahne, W. Kroontje, Soil Sci. Soc. Am. Proc. 37 (1973) 838.
[22] J.I. Drever, The Geochemistry of Natural Waters, Prentice Hall, New York, 1997.
[23] J.J. Rytuba, Sci. Total Environ. 260 (2000) 57.
[24] D.K. Nordstrom, C.N. Alpers, C.J. Ptacek, D.W. Blowes, Environ. Sci. Technol. 34 (2000) 254.
[25] M.A. Ali, D.A. Dzombak, Geochim. Cosmochim. Acta 60 (1996) 5045.
[26] D. Sarkar, M.E. Essington, K.C. Misra, Soil Sci. Soc. Am. J. 64 (2000) 1968.
[27] D. Sarkar, M.E. Essington, K.C. Misra, Soil Sci. Soc. Am. J. 63 (1999) 1626.
[28] P. Thanabalasingam, W.F. Pickering, Environ. Pollut. B 10 (1985) 115.
[29] J.R. Bargar, P. Persson, G.E. Brown Jr., J. Phys. IV C2 (1997) 825.
[30] G.A. Waychunas, G.E. Brown, Adv. X-Ray Anal. 37 (1994) 607.
[31] G.N. George, I.J. Pickering, EXAFSPAK, a Suite of Computer Programs for the Analysis of X-Ray Absorption Spectra, Stanford Synchrotron Radiation Laboratory, 1995.
[32] S.I. Zabinsky, J.J. Rehr, A. Ankudinov, R.C. Albers, M.J. Eller, Phys. Rev. B Condens. Matter Mater. Phys. 52 (1995) 2995.
[33] C. Tiffreau, J. Lutzenkirchen, P. Behra, J. Colloid Interface Sci. 172 (1995) 82, doi:10.1006/jcis.1995.1228.
[34] M.S. Gustin, H. Biester, C.S. Kim, Atmos. Environ. 36 (2002) 3241.
[35] C.R. Collins, D.M. Sherman, K.V. Ragnarsdottir, J. Colloid Interface Sci. 219 (1999) 345, doi:10.1006/jcis.1999.6464.
[36] S. Jayanetti, R.A. Mayanovic, A.J. Anderson, W.A. Bassett, I.M. Chou, J. Chem. Phys. 115 (2001) 954.
[37] I. Berrodier, F. Farges, M. Benedetti, G.E. Brown Jr., J. Synch. Radiat. 6 (1999) 651.
[38] N.J. Calos, H.L. Kennard, R.L. Davis, Z. Kristallogr. 187 (1989) 305.
[39] C.J. Chisholm-Brause, K.F. Hayes, A.L. Roe, G.E. Brown Jr., G.A. Parks, J.O. Leckie, Geochim. Cosmochim. Acta 54 (1990) 1897.
[40] J.R. Bargar, G.E. Brown Jr., G.A. Parks, Geochim. Cosmochim. Acta 61 (1997) 2617.
[41] R.S. Zhou, R.L. Snyder, Acta Crystallogr. Sect. B 47 (1991) 617.
[42] C. Dyer, P.J. Hendra, W. Forsling, M. Ranheimer, Spectrochim. Acta Part A 49 (1993) 691.
[43] E. Laiti, P. Persson, L.O. Ohman, Langmuir 14 (1998) 825.
[44] W. Stumm, Chemistry of the Solid–Water Interface: Processes at the Mineral–Water and Particle–Water Interface in Natural Systems, Wiley, New York, 1992.
[45] L.M. He, L.W. Zelazny, V.C. Baligar, K.D. Ritchey, D.C. Martens, Soil Sci. Soc. Am. J. 61 (1997) 784.
[46] S.S.S. Rajan, Soil Sci. Soc. Am. J. 42 (1978) 39.
[47] K. Aurivillius, Acta Crystallogr. 9 (1956) 685.
[48] A.E. Martell, R.M. Smith, Critical Stability Constants, Plenum, New York, 1976.